



---

RESEARCH ARTICLE

---

**PRODUCTION and CHARACTERIZATION of GELATIN FUNCTIONALIZED  
HYDROXYAPATITE COMPOSITE MICROSPHERES for BIOMEDICAL APPLICATIONS**

Fatih Erdem BAŞTAN \* 

Thermal Spray Research and Development Lab. (SAU-TESLAB), Metallurgical and Materials Engineering, Engineering Faculty, Sakarya University, Sakarya, Turkey

**ABSTRACT**

In this study, composite hydroxyapatite (HA)-gelatin microspheres (SD-HA-Gel) were produced for bone substitution applications. The polymer network within the HA matrix would be facilitated as a drug carrier system and can develop the cell-microsphere interactions due to the excellent biological properties of gelatin. Gelatin functionalized HA microspheres and bare HA granules (as a reference) with 8 µm average size were produced by spray drying process. The morphology, thermal properties, chemical and phase structure of the produced powders were analyzed by SEM, TG-DTA, FTIR and XRD methods. SD-HA-Gel microspheres presented spherical morphology and hollow/core-shell cross-section and consisted of HA nanoparticles and gelatin molecules together according to the SEM, FTIR and XRD studies. Thermal analyze results showed that gelatin evolved from the microspheres at ~300 °C. The effect of gelatin on the crystallization and high temperature stability of HA was studied by XRD analysis and Rietveld Refinement investigations. Gelatin was released from the microspheres after immersion for 14 days in phosphate buffer saline (PBS) solution.

**Keywords:** Functionalized Hydroxyapatite, Gelatin, Spray Drying, Rietveld Refinement

---

**1. INTRODUCTION**

Calcium phosphate (CaP) family members, such as hydroxyapatite and tricalcium phosphate having various Ca/P ratios, are commonly used bioactive ceramics owing to their outstanding biological properties. Hydroxyapatite (HA,  $\text{Ca}_{10}(\text{PO}_4)_6(\text{OH})_2$ ), resembling the main component of bone and teeth, has been emerged for decades owing to the capability to bond to the host tissue, osteointegration, osteoconduction, and etc. Despite its superior features, the inherent brittle nature of HA limits its usage in load-bearing applications; therefore, it can be used as a small defect size bone filler, orthopedic coating and drug carrier [1–6].

HA is further functionalized via therapeutic ion substitutions and blending with bioresorbable polymers.  $\text{Sr}^{2+}$  [7],  $\text{Zn}^{2+}$  [8],  $\text{Ag}^+$  [9], and recently a combination of multiple ions [10] were introduced into the HA crystal, which may alter the physical structure of HA and ultimately develop biological or mechanical properties [11, 12]. Addition of a biodegradable polymer (collagen, chitosan, PLLA) also enhances the biological features of the bioceramics such as biocompatibility, biosorption and cell affinity [13–15]. Bioceramics-especially CaPs- can be combined with biodegradable polymers to mimic the organic and inorganic components of bone [16]. Moreover, the abundant surface  $\text{OH}^-$  and  $\text{Ca}^{+2}$  ions provide nanostructured CaPs for loading a drug or gene. CaPs can be arranged as targeting nanocarriers through surface functionalization [17].

Gelatin (Gel), being denatured collagen, stimulates cellular adhesion, proliferation and differentiation [18]. The RGD sequence (tripeptide sequence) of gelatin interacts with the extracellular matrix proteins of bone and improves osteoblast adhesion and mineralization [19, 20]. Gelatin shows superior properties

such as good biodegradation, biocompatibility, availability, low cost and can be used safely in biomedicine [21]. HA is a favorable filler to gelatin matrix, and HA-gelatin composites are proposed as a bone substitute material due to good cell adhesion and proliferation [22]. Fang et al. [23] prepared stromal cell derived factor 1 added biomimetic HA-gelatin microspheres and found that the microspheres enhanced the alveolar bone regeneration. Chen et al [24] fabricated chitosan-gelatin-HA core-shell nanofibers to mimic the extracellular matrix of bone and observed that the composite nanofibers improved the osteoblast cells growth and gelatin incorporation increased the hydroxyapatite mineralization on the nanofibers. Hikmawati et al. [25] produced streptomycin loaded gelatin/hydroxyapatite injectable bone substitute material that was nontoxic to BHK-21 fibroblast and hepatocyte cells and presented antibacterial activity against *S. aureus*.

Spray drying (SD) is a versatile tool to produce HA granules to be used as a feedstock in thermal spraying [26] dental resin filler [27] protein [28] and drug [29] carries. In this technique, a prepared slurry was dried as a free-flowing powder, granule or agglomerate [30]. During the process, the slurry is atomized and subsequently dried in a hot chamber and finally is collected in a jar as a dried product [26]. Normally, polymers are utilized in the spray drying process to bind the particles within the spray dried granules together against disintegration. Polymers provides mechanical strength to the granules and evolves during post sintering process. More recently, biopolymers have been employed in the spray drying of HA to further functionalize the granules. SD facilitates to produce composite polymer-HA granules such as chitosan-HA [31],  $\epsilon$ -polylysine-HA [32], PVA-HA [33].

To the best of the author's knowledge, there have been limited studies on spray drying of HA-Gelatin microspheres. Chang [34] produced HA-Gelatin composite via spray precipitation method. Bielefeldt et al. [35] fabricated compressed blocks via spray-dried 20% gelatin incorporated HA microgranules and investigated flexural strength. Sun and Lu [36] formulated HA-gelatin via SD method; however, gelatin used as a pore-forming agent and removed through thermal treatment. In this study, SD-HA-Gelatin composite granules were produced to be used potentially as a bone substitute material with drug loading capability. The spray-dried microspheres were analyzed in terms of morphology, phase and chemical structure and thermal behavior. The gelatin could be further loaded with a drug or therapeutic ions. The gelatin network within the composite microgranules would not only develop the biological properties of HA but deliver loaded drugs/therapeutic ions into the damaged tissues.

## 2. MATERIALS and METHODS

Experimental work includes three main parts: 1. Synthesis of HA nanoparticles via precipitation, 2: Spray drying of HA and HA-gelatin (HA-Gel) composite microgranules and 3: Characterization of the microparticles.

### 2.1. Synthesis of HA Nanoparticles

Pure HA nanoparticles were synthesized via precipitation as described at our previous study [26]. Summarily, individual  $\text{Ca}(\text{NO}_3)_2 \cdot 4\text{H}_2\text{O}$  (98%, Merck) and  $(\text{NH}_4)_2\text{HPO}_4$  (98%, Merck) aqueous solutions were prepared and afterwards  $(\text{NH}_4)_2\text{HPO}_4$  solution was poured into the  $\text{Ca}(\text{NO}_3)_2$  solution. The pH was adjusted to 10.75 by  $\text{NH}_4\text{OH}$  solution and prepared HA suspension were mechanically stirred for 24 h at room temperature and precipitated for another 24 h. The HA wet cake was filtered and washed several times with de-ionized water and the nanoparticles were directly used in the spray drying process.

### 2.2. Spray Drying of HA and HA-Gelatin microgranules

Producing of bare HA microgranules: A slurry containing 5 wt. % HA nanoparticles was peristaltically pumped in a two-fluid external nozzle and atomized via pressured air into the hot spray dryer chamber

(Nubilos) according to the parameters in Table 1. Dried product (in this case bare HA) was collected at the bottom of the chamber in a glass jar.

**Table 1.** Spray drying parameters for producing of HA and SD-HA-Gel microspheres

Inlet temperature (°C)	Outlet temperature (°C)	Atomization pressure (bar)	Feeding rate (rpm)	HA rate (wt. %)
180	90	3	10	5

**Producing of HA-Gel microgranules:** 5 wt. % gelatin was dissolved in 1 vol. % acetic acid aqueous solution at 40 °C. Then, prepared gelatin solution was poured into the HA slurry and mixed for 1 h at room temperature. Finally, HA-Gel slurry involving 5 wt. % HA nanoparticles and 5 wt. gelatin was spray dried with the same parameters in Table 1. The producing of gelatin functionalized HA composite granules were schematized in Figure 1.

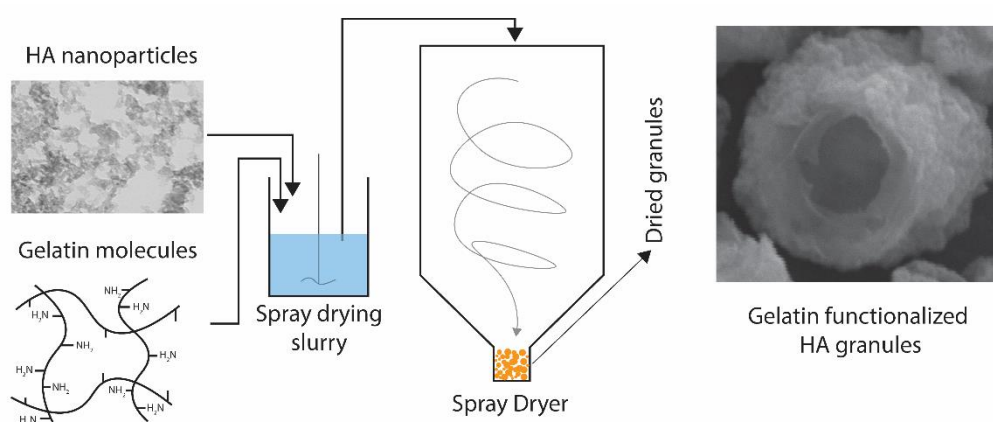


**Figure 1.** Schematic illustration of the producing route for gelatin functionalized HA granules

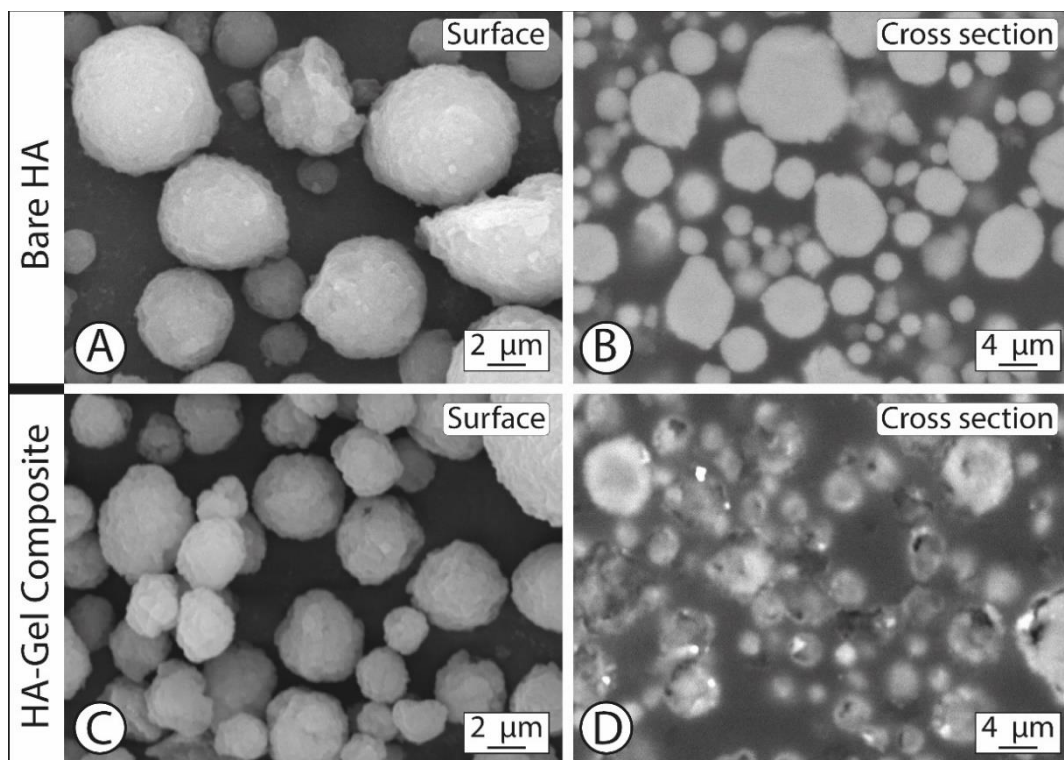
### 2.3. Characterization of the Granules

The surface and cross section morphology of the granules were monitored by scanning electron microscope (SEM, Tescan Vega II). For cross-section SEM investigations, the granules were embedded in an epoxy resin and polished via a cloth containing 1  $\mu\text{m}$   $\text{Al}_2\text{O}_3$  particles. The elemental mapping was applied on the embedded granules by energy dispersive X-ray (EDX, Bruker) spectroscopy attached at the SEM. The chemical structure of the granules was analyzed by Fourier transform infrared spectroscopy (FTIR, Shimadzu IRAffinity-1S). The transmittance mode was employed at FTIR with 4  $\text{cm}^{-1}$  resolution. The thermal behavior of the granules was examined by simultaneous thermogravimetric (TG) and differential thermal analyzer (DTA, Shimadzu DTG-60). The granules were heated up to 1500 °C at a 5 °C/min ramping rate in the air atmosphere. The spray dried samples were directly used in the thermal analyze experiments without any further drying. The crystal structure of the spray dried and heat treated granules was analyzed by X-ray diffraction analysis (XRD, Panalytical Cu  $K\alpha$  Empyrean Diffractometer). The diffractometer operated at 45kV and 40mA and data collected at a step size and time of 0.026° and 22 s, respectively. The size distribution of the granules was measured by a dry laser particle size analyzer (Microtrac S3500). To analyze the degradation behavior of the gelatin, 200 mg SD-HA-Gel composite granules were directly immersed in the 50 mL of phosphate buffered saline (PBS) solution at 37 °C (pH 7.4) for 14 d. 1 PBS tablet (Sigma) was dissolved in 200 mL of deionized water according to the supplier recipe. After 14 d immersion, the granules were taken from the solution, dried in an oven, and characterized by FTIR to analyze the releasing of gelatin by controlling the change

of gelatin's characteristic bands and SEM to visualize possible morphology change after liberating of the gelatin molecules.

### 3. RESULTS and DISCUSSION

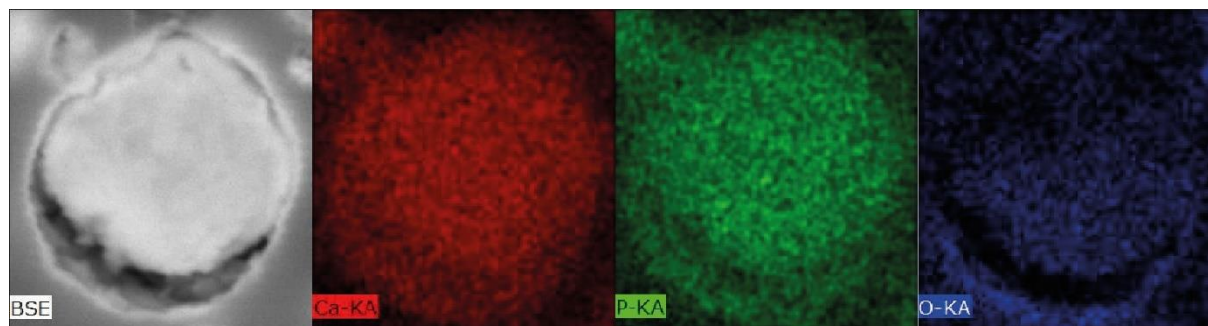
It is well known that hollow, donut and spherical microgranules can be formulated via spray drying process [37]. Figure 2 illustrates the surface and cross-section SEM images of bare HA and SD-HA-Gel composite microgranules. Spray-dried HA microgranules (SD-HA) had spherical surface morphology and solid cross-section. Generally, polymer binders were used in the spray drying procedure to increase the mechanical integrity of the granules. Ben et al. [38] observed that PVB modification above 0.5 wt. % enhanced the mechanical integrity of the spray dried tri-calcium phosphate granules. In this study, no disaggregated pure HA granule was observed that may be attributed to the higher surface energy of the nanoparticles providing the energy to preserve the integrity of the granules. Both HA and SD-HA-Gel granules presented identical size distributions (d10: 2.5  $\mu\text{m}$ , d50: 8  $\mu\text{m}$  and d90: 18  $\mu\text{m}$ ). I selected spray drying and slurry parameters to produce granules with relatively smaller sizes to suspend them in the solutions with ease. SD-HA-Gel composite microspheres (SD-HA-Gel) commonly presented spherical morphology, and some hollow microspheres can also be seen. However, the cross-section microstructure of SD-HA-Gel differed from the SD-HA, i.e., it was predominantly composed of hollow microspheres. The spherical morphology of the spray dried granules can be transformed to hollow, donut, apple like morphologies by the relatively higher binder amount [16,38]. During the drying process, water and binder (in this case gelatin) move toward to the atomized droplet surface. Afterwards, the particles and binder form a dense shell around the droplet and left an internal void. The difference of pressure between the ambient atmosphere and the internal void causes to collapse one part of the granule and consequently, a hollow granule forms [39].



**Figure 2.** SEM images of A-B) Bare HA and C-D) SD-HA-Gel composite microspheres

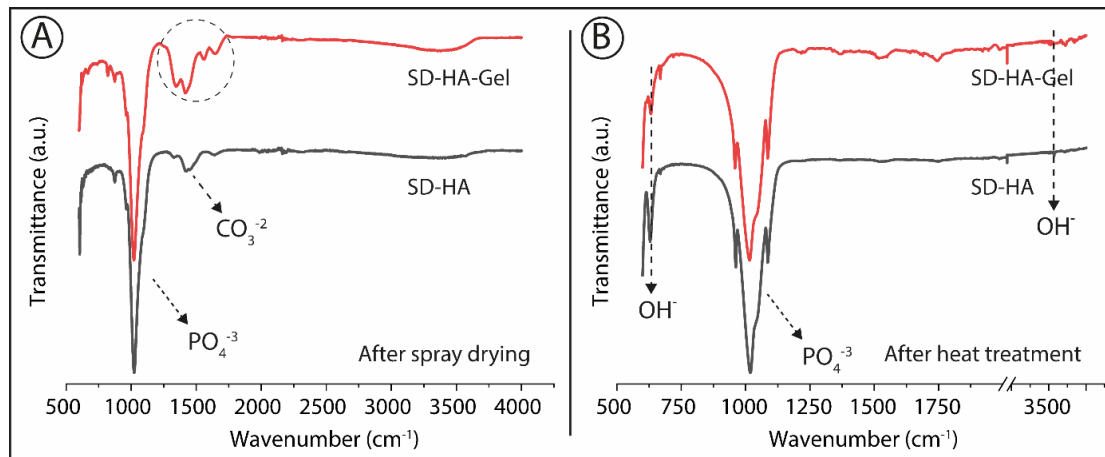
Some of the SD-HA-Gel had a core-shell structure that the microgranule composed of a shell at the outer surface and a dense inherent core (Figure 3) The EDX mapping shows that Ca, P and O were enriched

at the outer surface and the core of the microgranules. The formation of this morphology can be attributed to the segregation of the polymer and ceramic particles (in this case, gelatin and HA) to the outer surface of the droplet during spray drying [40]. Consequently, it can be inferred from Figure 2 and Figure 3 that the introducing of gelatin into the HA slurry led to change the cross-section morphology to a mix of hollow and core-shell microstructures. Sinha et al. [41] pointed out the formation of the ruptured granules with thicker shell by the breaking of the granules due to the increased internal pressure and the development of the hollow microspheres by the porous structure of the shell.



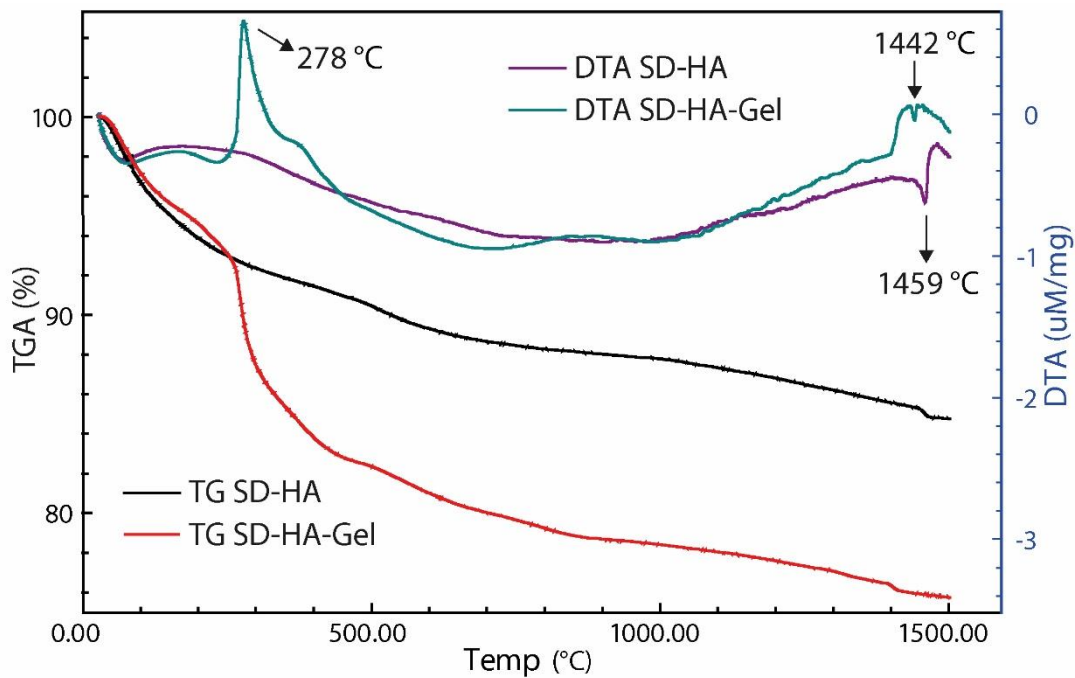
**Figure 3.** SEM cross-section morphology and elemental mapping images

Figure 4 demonstrates the FTIR spectra of the spray-dried and heat-treated microgranules. It was investigated that FTIR spectrum of the spray-dried bare HA microgranules matches with that of the hydroxyapatite: The bands at around 603, 960, and 1020  $\text{cm}^{-1}$  were attributed to the P-O bands, whereas, the peaks at 630 and 3572  $\text{cm}^{-1}$  were assigned to the hydroxyl group. A broad water band at about 3400  $\text{cm}^{-1}$  showed that spray dried bare HA granules were not completely dried. The carbonate peaks around 870  $\text{cm}^{-1}$ , and between 1400-1550  $\text{cm}^{-1}$  appeared due to the synthesis procedure and disappeared after the heat treatment (Figure 4B) [10,42–44]. SD-HA-Gel microgranules had not only similar P-O bands with those of neat HA but also new peaks between 1225-1750  $\text{cm}^{-1}$  (within the dotted circle in Figure 4A) that can appear due to the gelatin incorporation. The peaks at ~1650  $\text{cm}^{-1}$  (Amide-I) and 1540  $\text{cm}^{-1}$  (Amide-II), were assigned to the C=O stretching, N-H bending and C-H stretching, while, the peak at 1450  $\text{cm}^{-1}$  corresponded to the C-O stretching of gelatin molecules [45,46]. Furthermore, it was observed that the intensities of carbonate band at around 1400  $\text{cm}^{-1}$  and water band at about 3400  $\text{cm}^{-1}$  were relatively higher in the FTIR spectrum of SD-HA-Gel microgranules. FTIR results proved that spray-dried HA-Gel microgranules (SD-HA-Gel) contain HA particles and gelatin molecules. Most of the gelatin evolved from the SD-HA-Gel microstructure by the heat treatment at 1000  $^{\circ}\text{C}$ , as expected (Figure 4B) [36]. It was investigated that the intensity of hydroxyl band at 630  $\text{cm}^{-1}$  for SD-HA-Gel microgranules decreased after the heat treatment. Hence, it can be concluded that gelatin incorporation into the microgranules caused further dehydroxylation of hydroxyapatite crystals. Similarly, Shu et al. [47] reported that introducing of gelatin during the precipitation process of HA reduced in the intensity of the hydroxyl bands.



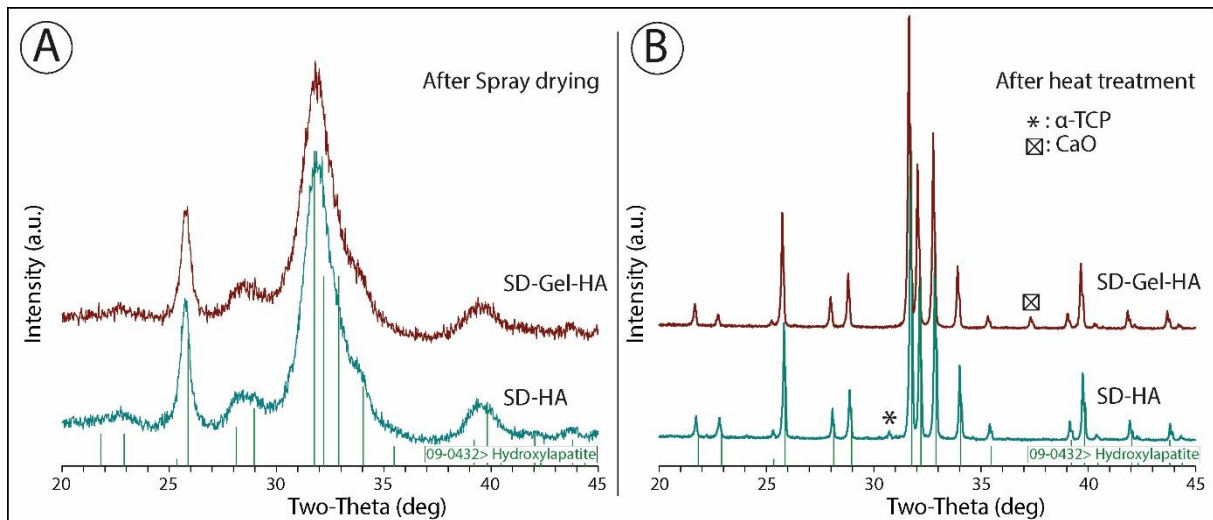
**Figure 4.** FTIR spectra of micro granules A) after spray drying and B) after heat treatment at 1000 °C

Figure 5 shows the TG and DTA profiles of the SD-HA and SD-HA-Gel microgranules. Three main sections of weight loss can be seen in the TG of SD-HA. The first mass loss up to 500 °C corresponded to the removal of physically adsorbed water, lattice water and synthesis by-product. The second mass loss-up to 1400 °C- can be attributed to the decarbonization (evolving of  $\text{CO}_3^{2-}$ ) and gradual dehydroxylation of the apatite structure. The endothermic DTA peak at 1459 °C demonstrated that produced SD-HA decomposed to other calcium phosphates (TCP and TTCP) at this temperature [7,26,48]. The thermal behavior of the SD-HA-Gel up to 250 °C was quite similar to that of the SD-HA. However, above this temperature up to 450 °C, a sharp mass loss can be noticed (Figure 5). Normally, 5 wt. % gelatin introduced into the HA granules, however, the mass loss difference between the pure SD-HA and SD-HA-Gel was approximately 10 wt. %. As mentioned in the FTIR section, SD-HA-Gel granules involved more water molecules and carbonate groups than pure HA. However, the higher mass loss at the temperature range 250 °C-450 °C can be assigned to the liberation of water molecules due to the fact that carbonate groups generally evolved from the HA at relatively higher temperatures [49]. The higher amount of water molecules could be retained in the granules by adsorbing to the gelatin molecules. On the other hand, the gelatin film formed on the granules during spray drying may retard the migration of the water from the inner side of the granules. There was an exothermic peak at this temperature range composed two integrated peaks at 278 °C and at ~350 °C in DTA graphic of SD-HA-Gel. This mass loss and the exothermic peak can be assigned to the burning and releasing of the gelatin in the microgranules [50,51]. It could be suggested that at the first stage, most of the gelatin molecules absorbed on the SD-HA-Gel microgranules evolved and then the residual gelatin inside the granules released at relatively higher temperatures. The TG and DTA profiles of SD-HA-Gel was similar to those of SD-HA above 450 °C. Solely, it was investigated that SD-HA-Gel microgranules lost more mass than pure HA at the temperature ranges 500 °C-900 °C due to the releasing higher amount of carbonate groups. The incorporation of the gelatin into the HA slightly reduced the decomposition temperature from 1459 °C to 1442 °C. It can be concluded from the TG-DTA and FTIR results that gelatin can be successfully incorporated into the microgranules.



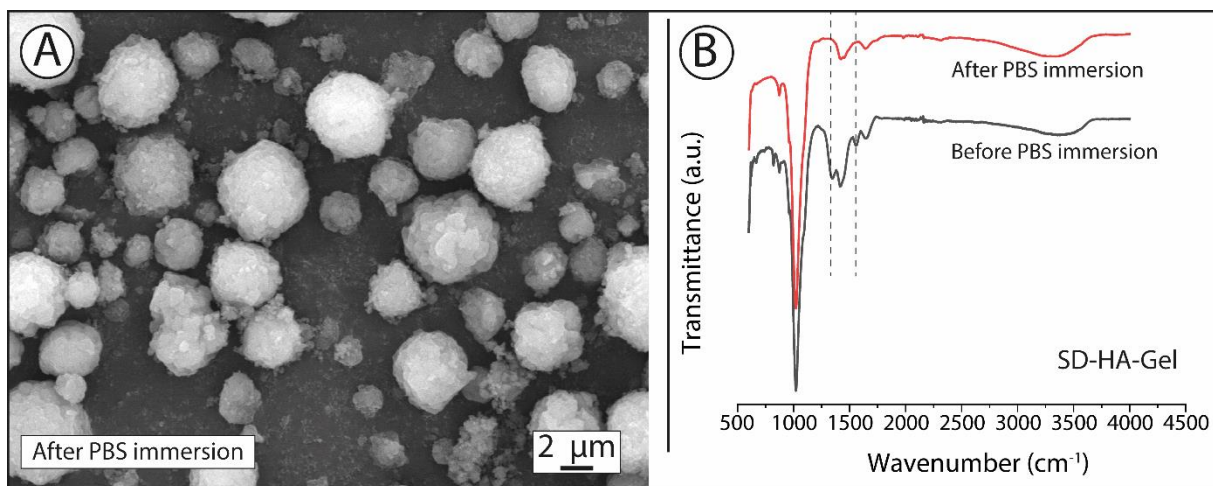
**Figure 5.** TG and DTA profiles of the spray-dried granules

Figure 6 illustrates the XRD spectra of the spray-dried and heat-treated SD-HA and SD-HA-Gel microgranules. The XRD spectrum of SD-HA (Figure 6A) presented characteristic diffraction peaks at  $2\theta$  25.4°, 31.7°, 34° and 39.8° matches with the (002), (211), (202) and (310) crystalline planes of HA phase (PDF 09-432 XRD card), respectively [52,53]. In the available literature, it was reported that the effect of gelatin on the crystal structure of the HA was multifold: Gelatin reduced the crystallinity/crystal size of the HA nanoparticles when it was added during the precipitation of HA [54]. Otherwise, mixing of the gelatin directly with HA nanoparticles showed no effect on the crystal structure of the HA [55]. In this study, gelatin was incorporated in the spray drying slurry containing HA nanoparticles. Therefore, gelatin incorporation did not affect the crystal structure of HA that SD-HA-Gel had exactly the same XRD spectra with that of the SD-HA (Figure 6A). The precipitated HA had fine crystallites/ low crystallinity. Hence, the XRD spectra of SD-HA and SD-HA-Gel had broad diffraction peaks [56]. SD-HA and SD-HA-Gel presented ~5 nm average crystal size calculated by the Rietveld refinement analysis. The heat treatment at 1000 °C increased the crystallite sizes/crystallinity and thus, the diffraction peaks were sharpened (Figure 6B). The XRD spectra of the heat-treated SD-HA and SD-HA-Gel were well-matched with the crystalline HA (PDF 09-432). Furthermore, a peak corresponding to the  $\alpha$ -TCP phase was determined in the XRD pattern of the SD-HA, whereas CaO phase was monitored in the XRD spectrum of SD-HA-Gel granules. SD-HA was composed of 96.7% HA and 3.3% TCP, respectively according to the Rietveld Refinement analysis. It is well-known that precipitated carbonated apatite (calcium deficient HA) is commonly decomposed to a mixture of HA and TCP at elevated temperatures [57]. However, SD-HA-Gel microgranules consisted 98.9% HA and 1.1% CaO phases. The incorporation of gelatin influenced the crystallization and changed the thermal decomposition behavior of the precipitated HA to a different manner due to the possible interaction of Ca ions with gelatin molecules [47].



**Figure 6.** XRD spectra of the A) spray-dried and B) heat-treated microgranules

Figure 7 demonstrates the surface SEM image and FTIR spectrum of the SD-HA-Gel after immersion in PBS solution for 14 days. It can be seen from Figure 7A that some of the nano HA particles were disintegrated from the granule surface due to the dissolution of the gelatin into the PBS from the outer surface of the granules. Figure 7B shows the FTIR spectra of the SD-HA-Gel before and after immersion in PBS solution. Some of the FTIR peaks vanished after the immersion in PBS solution for 14 days when compared to those of spray-dried HA-Gel microgranules. These FTIR peaks were related to the gelatin molecules, and thus it was determined that gelatin was released into the PBS solution. The release of the gelatin into the physiological medium may develop the biological properties of the microgranules. Moreover, gelatin can be used as a matrix for drugs/genes or therapeutic ions, which can provide a controlled local release of drugs or therapeutic ions with the dissolution of gelatin. For instance, Sirivat and Paradee [58] utilized gelatin-coated  $Fe_3O_4$  nanoparticles for cancer drug mercaptopurine delivery. Rahmanian et al. [59] prepared gelatin-tricalcium phosphate scaffold for loading with the zoledronic acid drug.



**Figure 7.** A) SEM micrograph and B) FTIR of the microgranules after the immersion for 14 days

#### **4. CONCLUSION**

In this study, gelatin functionalized hollow and core/shell hydroxyapatite (SD-HA-Gel) microspheres were produced by the spray drying process. The formation of hollow and core/shell morphology by spray drying was studied. The granules were characterized in terms of surface and cross-section morphology, thermal behavior, and chemical structure. Moreover, the effect of gelatin incorporation to the crystallization and thermal stability of HA was investigated by XRD and Rietveld Refinement analysis. The conclusions about this study are listed below:

1. FTIR and TG-DTA results proved that SD-HA-Gel microspheres were composed of HA and gelatin together and gelatin evolved from the microspheres between 250 °C-450 °C.
2. Gelatin incorporation affected the crystal structure of HA insignificantly according to the XRD results. After heat treatment at 1000 °C, both SD-HA and SD-HA-Gel microspheres presented dominantly crystalline apatite structure. The effect of gelatin on the thermal stability and decomposition of HA should be further evaluated.
3. Most of the gelatin in the SD-HA-Gel microspheres was released into the PBS solution after the immersion for 14 days.
4. The in-vitro bioactivity (simulated body fluid test and cell tests) should be further evaluated. A drug or therapeutic ion would be loaded to gelatin matrix, and the drug release capability of the microspheres can be investigated at future studies.
5. The amount of gelatin would be adjusted in future studies to show the effect of gelatin loading on the morphology, drug loading and releasing capacity and the in-vitro bioactivity of the granules.

#### **ACKNOWLEDGEMENTS**

The author would like to thank Sakarya University Thermal Spray Research and Development Laboratory, especially the head Prof. Fatih Üstel for providing the entire analyzing equipment. This work was partly supported by The Scientific and Technological Research Council of Turkey, TÜBİTAK (Project no: 1919B011801595) and the author would like to give gratitude to Mat. Eng. Hilmi Tunahan Eligül and Sergen Belit for their assistance on producing and characterization of HA/gelatin microspheres and Dr. Egemen Avcu and Dr. Muhammad Atiq Ur Rehman for helping on writing process of the paper.

#### **CONFLICT OF INTEREST**

The author stated that there are no conflicts of interest regarding the publication of this article.

#### **REFERENCES**

- [1] Tite T, Popa A-C, Balescu LM, Bogdan IM, Pasuk I, Ferreira JMF, Stan GE. Cationic Substitutions in Hydroxyapatite: Current Status of the Derived Biofunctional Effects and Their In Vitro Interrogation Methods. *Materials* 2018; 11: 2081.
- [2] Siddiqui H, Pickering K, Mucalo M, Siddiqui HA, Pickering KL, Mucalo MR. A Review on the Use of Hydroxyapatite-Carbonaceous Structure Composites in Bone Replacement Materials for Strengthening Purposes. *Materials* 2018; 11: 1813.
- [3] Safi S, Karimzadeh F, Labbaf S. Mesoporous and hollow hydroxyapatite nanostructured particles as a drug delivery vehicle for the local release of ibuprofen. *Mater Sci Eng C* 2018; 92: 712–719.

- [4] Medeiros SJ, Oliveira AM, Carvalho JO de, Ricci R, Martins M do CC, Rodrigues BVM, Webster TJ, Viana BC, Vasconcellos LMR, Canevari RA, Marciano FR, Lobo AO. Nanohydroxyapatite/Graphene Nanoribbons Nanocomposites Induce in Vitro Osteogenesis and Promote in Vivo Bone Neof ormation. *ACS Biomater Sci Eng* 2018; 4: 1580–1590.
- [5] Diaz-Rodriguez P, Sánchez M, Landin M. Drug-Loaded Biomimetic Ceramics for Tissue Engineering. *Pharmaceutics* 2018; 10: 272.
- [6] Bose S, Ke D, Sahasrabudhe H, Bandyopadhyay A. Additive manufacturing of biomaterials. *Prog Mater Sci* 2018; 93: 45–111.
- [7] Özbek YY, Baştan FE, Üstel F. Synthesis and characterization of strontium-doped hydroxyapatite for biomedical applications. *J Therm Anal Calorim* 2016; 125: 745–750.
- [8] Robles-Águila MJ, Reyes-Avenidaño JA, Mendoza ME. Structural analysis of metal-doped (Mn, Fe, Co, Ni, Cu, Zn) calcium hydroxyapatite synthesized by a sol-gel microwave-assisted method. *Ceram Int* 2017; 43: 12705–12709.
- [9] Baştan FE, Özbek YY. Producing antibacterial silver-doped hydroxyapatite powders with chemical precipitation and reshaping in a spray dryer. *Mater Tehnol* 2013; 47: 431–434.
- [10] Lowry N, Brolly M, Han Y, McKillop S, Meenan BJ, Boyd AR. Synthesis and characterisation of nanophase hydroxyapatite co-substituted with strontium and zinc. *Ceram Int* 2018; 44: 7761–7770.
- [11] Graziani G, Boi M, Bianchi M, Graziani G, Boi M, Bianchi M. A Review on Ionic Substitutions in Hydroxyapatite Thin Films: Towards Complete Biomimetism. *Coatings* 2018; 8: 269.
- [12] Ratnayake JTB, Mucalo M, Dias GJ. Substituted hydroxyapatites for bone regeneration: A review of current trends. *J Biomed Mater Res B Appl Biomater* 2016; 105: 1285–1299.
- [13] Liang C, Luo Y, Yang G, Xia D, Liu L, Zhang X, Wang H. Graphene Oxide Hybridized nHAC/PLGA Scaffolds Facilitate the Proliferation of MC3T3-E1 Cells. *Nanoscale Res Lett* 2018; 13: 15.
- [14] Alizadeh-Osgouei M, Li Y, Wen C. A comprehensive review of biodegradable synthetic polymer-ceramic composites and their manufacture for biomedical applications. *Bioact Mater* 2018; 4: 22–36.
- [15] Yu P, Bao R-Y, Shi X-J, Yang W, Yang M-B. Self-assembled high-strength hydroxyapatite/graphene oxide/chitosan composite hydrogel for bone tissue engineering. *Carbohydr Polym* 2017; 155: 507–515.
- [16] Ruphuy G, Saralegi A, Lopes JC, Dias MM, Barreiro MF. Spray drying as a viable process to produce nano-hydroxyapatite/chitosan (n-HAp/CS) hybrid microparticles mimicking bone composition. *Adv Powder Technol* 2016; 27: 575–583.
- [17] Qi C, Lin J, Fu L-H, Huang P. Calcium-based biomaterials for diagnosis, treatment, and theranostics. *Chem Soc Rev* 2018; 47: 357–403.

- [18] Yan Y, Zhang X, Mao H, Huang Y, Ding Q, Pang X. Hydroxyapatite/gelatin functionalized graphene oxide composite coatings deposited on TiO<sub>2</sub> nanotube by electrochemical deposition for biomedical applications. *Appl Surf Sci* 2015; 329: 76–82.
- [19] Nair M, Nancy D, Krishnan AG, Anjusree GS, Vadukumpully S, Nair SV. Graphene oxide nanoflakes incorporated gelatin–hydroxyapatite scaffolds enhance osteogenic differentiation of human mesenchymal stem cells. *Nanotechnology* 2015; 26: 161001.
- [20] Rehman MAU, Munawar MA, Schubert DW, Boccaccini AR. Electrophoretic deposition of chitosan/gelatin/bioactive glass composite coatings on 316L stainless steel: A design of experiment study. *Surf Coat Technol* 2019; 358: 976–986.
- [21] Liu H, Cheng J, Chen F, Bai D, Shao C, Wang J, Xi P, Zeng Z. Gelatin functionalized graphene oxide for mineralization of hydroxyapatite: biomimetic and in vitro evaluation. *Nanoscale* 2014; 6: 5315–5322.
- [22] Lian H, Zhang L, Meng Z. Biomimetic hydroxyapatite/gelatin composites for bone tissue regeneration: Fabrication, characterization, and osteogenic differentiation in vitro. *Mater Des* 2018; 156: 381–388.
- [23] Fang C-H, Lin Y-W, Lin F-H, Sun J-S, Chao Y-H, Lin H-Y, Chang Z-C. Biomimetic Synthesis of Nanocrystalline Hydroxyapatite Composites: Therapeutic Potential and Effects on Bone Regeneration. *Int J Mol Sci* 2019; 20: 6002.
- [24] Chen P, Liu L, Pan J, Mei J, Li C, Zheng Y. Biomimetic composite scaffold of hydroxyapatite/gelatin-chitosan core-shell nanofibers for bone tissue engineering. *Mater Sci Eng C* 2019; 97: 325–335.
- [25] Hikmawati D, Maulida HN, Putra AP, Budiati AS, Syahrom A. Synthesis and Characterization of Nanohydroxyapatite-Gelatin Composite with Streptomycin as Antituberculosis Injectable Bone Substitute. *Int J Biomater* 2019; 1–8.
- [26] Bastan FE, Erdogan G, Moskalewicz T, Ustel F. Spray drying of hydroxyapatite powders: The effect of spray drying parameters and heat treatment on the particle size and morphology. *J Alloys Compd* 2017; 724: 586–596.
- [27] Zhao S-N, Yang D-L, Wang D, Pu Y, Le Y, Wang J-X, Chen J-F. Design and efficient fabrication of micro-sized clusters of hydroxyapatite nanorods for dental resin composites. *J Mater Sci* 2019; 54: 3878–3892.
- [28] Stipnice L, Stepanova V, Narkevica I, Salma-Ancane K, Boyd AR. Comparative study of surface properties of Mg-substituted hydroxyapatite bioceramic microspheres. *J Eur Ceram Soc* 2018; 38: 761–768.
- [29] Yu M, Zhou K, Li Z, Zhang D. Preparation, characterization and in vitro gentamicin release of porous HA microspheres. *Mater Sci Eng C* 2014; 45: 306–312.
- [30] Murtaza Q, Stokes J, Ardhaoui M. Experimental Analysis of Spray Dryer Used in Hydroxyapatite Thermal Spray Powder. *J Therm Spray Technol* 2012; 21: 963–974.
- [31] Başargan T, Nasün-Saygılı G. Spray-Dried Mesoporous Hydroxyapatite–Chitosan Biocomposites. *Polym-Plast Technol Eng* 2015; 54: 1172–1183.

- [32] Stipniece L, Salma-Ancane K, Narkevica I, Juhnevica I, Berzina-Cimdina L. Fabrication of nanostructured composites based on hydroxyapatite and  $\epsilon$ -polylysine. *Mater Lett* 2016; 163: 65–68.
- [33] Stipniece L, Salma-Ancane K, Rjabovs V, Juhnevica I, Turks M, Narkevica I, Berzina-Cimdina L. Development of functionalized hydroxyapatite/poly(vinyl alcohol) composites. *J Cryst Growth* 2016; 444: 14–20.
- [34] Chang MC. Fluoride incorporation in hydroxyapatite/gelatin nanocomposite. *J Mater Sci Mater Med* 2008; 19: 2837–2843.
- [35] Bielefeldt N, Ploska U, Berger G, Heimann L. Rapidly resorbable, temporarily mechanically stable composites for bone replacement. *Key Eng Mater* 2009; 396–398: 469–472.
- [36] Sun R, Lu Y. Fabrication and characterization of porous hydroxyapatite microspheres by spray-drying method. *Front Mater Sci China* 2008; 2: 95–98.
- [37] Nandiyanto ABD, Okuyama K. Progress in developing spray-drying methods for the production of controlled morphology particles: From the nanometer to submicrometer size ranges. *Adv Powder Technol* 2011; 22: 1–19.
- [38] Ben Y, Zhang L, Wei S, Zhou T, Li Z, Yang H, Wang Y, Selim FA, Wong C, Chen H. PVB modified spherical granules of  $\beta$ -TCP by spray drying for 3D ceramic printing. *J Alloys Compd* 2017; 721: 312–319.
- [39] Bertrand G, Filiatre C, Mahdjoub H, Foissy A, Coddet C. Influence of slurry characteristics on the morphology of spray-dried alumina powders. *J Eur Ceram Soc* 2003; 23: 263–271.
- [40] Fu N, Wu WD, Wu Z, Moo FT, Woo MW, Selomulya C, Chen XD. Formation process of core-shell microparticles by solute migration during drying of homogenous composite droplets. *AIChE J* 2017; 63: 3297–3310.
- [41] Sinha A, Mishra T, Ravishankar N. Polymer assisted hydroxyapatite microspheres suitable for biomedical application. *J Mater Sci Mater Med* 2008; 19: 2009–2013.
- [42] Yao H-L, Hu X-Z, Bai X-B, Wang H-T, Chen Q-Y, Ji G-C. Comparative study of HA/TiO<sub>2</sub> and HA/ZrO<sub>2</sub> composite coatings deposited by high-velocity suspension flame spray (HVSFS). *Surf Coat Technol* 2018; 351: 177–187.
- [43] Hidalgo-Robatto BM, López-Álvarez M, Azevedo AS, Dorado J, Serra J, Azevedo NF, González P. Pulsed laser deposition of copper and zinc doped hydroxyapatite coatings for biomedical applications. *Surf Coat Technol* 2018; 333: 168–177.
- [44] Paul S, Pal A, Choudhury AR, Bodhak S, Balla VK, Sinha A, Das M. Effect of trace elements on the sintering effect of fish scale derived hydroxyapatite and its bioactivity. *Ceram Int* 2017; 43: 15678–15684.
- [45] Ahlawat J, Kumar V, Gopinath P. Carica papaya loaded poly (vinyl alcohol)-gelatin nanofibrous scaffold for potential application in wound dressing. *Mater Sci Eng C* 2019; 103: 109834.

- [46] Yin F, Lin L, Zhan S. Preparation and properties of cellulose nanocrystals, gelatin, hyaluronic acid composite hydrogel as wound dressing. *J Biomater Sci Polym Ed* 2019; 30: 190–201.
- [47] Shu C, Xianzhu Y, Zhangyin X, Guohua X, Hong L, Kangde Y. Synthesis and sintering of nanocrystalline hydroxyapatite powders by gelatin-based precipitation method. *Ceram Int* 2007; 33: 193–196.
- [48] Tõnsuaadu K, Gross K, Plūduma L, Veiderma M. A review on the thermal stability of calcium apatites. *J Therm Anal Calorim* 2012; 110: 647–659.
- [49] Sofronia AM, Baies R, Anghel EM, Marinescu CA, Tanasescu S. Thermal and structural characterization of synthetic and natural nanocrystalline hydroxyapatite. *Mater Sci Eng C* 2014; 43: 153–163.
- [50] Ran J, Hu J, Chen L, Shen X, Tong H. Preparation and characterization of gelatin/hydroxyapatite nanocomposite for bone tissue engineering. *Polym Compos* 2017; 38: 1579–1590.
- [51] Sanoop PK, Mahesh KV, Nampoothiri KM, Mangalaraja RV, Ananthakumar S. Multifunctional ZnO-biopolymer nanocomposite coatings for health-care polymer foams and fabrics. *J Appl Polym Sci* 2012; 126: E233–E244.
- [52] Pawlik A, Rehman MAU, Nawaz Q, Bastan FE, Sulka GD, Boccaccini AR. Fabrication and characterization of electrophoretically deposited chitosan-hydroxyapatite composite coatings on anodic titanium dioxide layers. *Electrochimica Acta* 2019; 307: 465–473.
- [53] Wei L, Yang H, Hong J, He Z, Deng C. Synthesis and structure properties of Se and Sr co-doped hydroxyapatite and their biocompatibility. *J Mater Sci* 2019; 54: 2514–2525.
- [54] Chao SC, Wang M-J, Pai N-S, Yen S-K. Preparation and characterization of gelatin–hydroxyapatite composite microspheres for hard tissue repair. *Mater Sci Eng C* 2015; 57: 113–122.
- [55] Kailasanathan C, Selvakumar N. Influence of alumina reinforcement on nano-hydroxyapatite/biopolymer composite for biomedical applications. *Int J Polym Anal Charact* 2016; 21: 554–562.
- [56] Kolmas J, Velard F, Jaguszewska A, Lemaire F, Kerdjoudj H, Gangloff SC, Kafalak A. Substitution of strontium and boron into hydroxyapatite crystals: Effect on physicochemical properties and biocompatibility with human Wharton-Jelly stem cells. *Mater Sci Eng C* 2017; 79: 638–646.
- [57] Champion E. Sintering of calcium phosphate bioceramics. *Acta Biomater* 2013; 9: 5855–5875.
- [58] Sirivat A, Paradee N. Facile synthesis of gelatin-coated Fe<sub>3</sub>O<sub>4</sub> nanoparticle: Effect of pH in single-step co-precipitation for cancer drug loading. *Mater Des* 2019; 181: 107942.
- [59] Rahmanian M, seyfoori A, Dehghan MM, Eini L, Naghib SM, Gholami H, Farzad Mohajeri S, Mamaghani KR, Majidzadeh-A K. Multifunctional gelatin–tricalcium phosphate porous nanocomposite scaffolds for tissue engineering and local drug delivery: In vitro and in vivo studies. *J Taiwan Inst Chem Eng* 2019; 101: 214–220.